Keywords: Turbocharging strategies, predictive thermodynamic combustion models, Ammonia/hydrogen marine engine, Diesel-gas mode

Turbocharging strategies to enable fuel-flexibility over a full operating map in a 4-stroke marine engine

Dr. Qiyan Zhou[1], Dr. Dirk Bergmann[1], Elmar Strittmatter[1], Herve Martin[1], Prof. Dr. Gianluca D'Errico[2], Alberto Ballerini[2]

(1) Accelleron c/o Turbo Systems Switzerland Ltd, (2) Department of Energy, Politecnico di Milano

https://doi.org/10.18453/rosdok_id00004636

Abstract

The use of alternative marine fuels is considered an important strategy to reduce the environmental and climate impacts of shipping. Among all the future fuels, ammonia has been gaining attention recently thanks to its potential to be carbon-free from production to combustion. There are a lot of attempts to use ammonia in the premixed Otto cycle, where a high compression ratio is used due to its high-octane rating, and hydrogen is added to compensate for its high ignition energy and low flame speed. A fuel-flexible ammonia-Diesel engine, where depending on prices or local regulations, the operators can decide to use ammonia in the gas mode or switch to conventional Diesel mode, is of great interest for maritime decarbonization, cost reduction, and enhancing reliability. In particular, Diesel fuel also provides a backup operation in case of gas feed interruption or component failure. However, the two working modes may differ in air requirement and exhaust temperature, which might add another layer of complexity in turbo-matching. To this end, the ultimate goal of this paper is to perform a comprehensive study on turbocharging strategies and provide a solution to enable optimal engine performance in both working modes.

In this paper, simulations are performed using ACTUS (Advanced Computation of TUrbocharging Systems), the Accelleron in-house software for large-bore engine simulation, in which advanced and predictive thermodynamic combustion models for both premixed and diffusive combustion developed by Politecnico di Milano have been included recently. Details of the combustion models will be first given, and then the model validation will be performed. In particular, a premixed combustion model based on the flamelet assumption will be used to simulate the natural gas engine considering the equivalence air-fuel ratio (ϕ), spark timing and load sweeps; a constant equivalence ratio multi-zone approach for diffusion flames will be validated along the nominal operating curve in a Diesel engine. Different turbocharging strategies will be investigated and compared to optimize the air supply system, which could enable fuel flexibility in ammonia–Diesel engines.

1. Introduction

The International Maritime Organization (IMO) has proposed a reduction of at least 70% in greenhouse gas (GHG) emissions from international shipping by 2040, with the ultimate goal of achieving net-zero shipping by around 2050 [1]. As a result, replacing conventional marine fuels with near-zero or net-zero GHG alternative fuels is inevitable and is being actively researched and developed. There have been many studies comparing the application of various alternative fuels in the marine sector: Stolz et al. [2] compared various alternative fuels such as hydrogen, ammonia, methane, and methanol and concluded that ammonia is the most balanced carbon-free fuel, while methanol is the most balanced carbonaceous fuel. Kanchiralla et al. [3] compared the lifecycle costs of using hydrogen, ammonia, and methanol as alternative fuels in three ships. They found that the use of ammonia and methanol fuel has the lowest lifecycle cost for all studied cases. In [4], Zhou et al. further highlighted ammonia as an ideal alternative fuel for future international shipping due to its low storage and transportation costs, as well as its well-established infrastructures. One of the possible approaches to burn ammonia in IC engine applications is the use of the Otto cycle, either through the spark ignition or a dual-fuel approach involving a small amount of highly reactive fuel, such as diesel [5]. Recognizing the variability of operational conditions and regulatory landscapes across different maritime regions, an ammonia-Diesel dual fuel engine is preferred, where depending on prices or local regulations, the operators can decide to use ammonia in the gas mode or switch to conventional Diesel mode, similar to [6]. This is of great interest for maritime decarbonization, cost reduction, and enhancing reliability, in particular, Diesel fuel also provides a backup operation in case of gas feed interruption or component failure. However, the two working modes may differ in air requirement and exhaust temperature, which might add another layer of complexity in turbo-matching. A comprehensive assessment of the turbocharging system will be essential to determine the optimal strategy for enabling fuel flexibility in such an ammonia-Diesel dual-fuel engine.

To assess different turbocharging strategies without incurring significant costs, advanced 1D-0D computational tools are crucial, where an accurate description of the combustion process is essential for a precise and detailed turbocharging study, especially for ammonia engines with limited experimental data. Over the years, various combustion models have been developed in different computational codes to simulate combustion in IC engines, ranging from fast and simple empirical relations such as the Wiebe or semi-empirical models [7], to more complex and capable thermodynamic models [8], [9]. Accelleron has a long tradition of developing simulation tools for turbocharged large engine system [10], and in 2012, it introduced its new simulation software, ACTUS (Advanced Computation of TUrbocharging Systems). Since then, a continuous development and improvement of the modeling capability of ACTUS has been carried out, and recently the advanced and predictive thermodynamic combustion models for both premixed and diffusive combustion developed by Politecnico di Milano have been included for investigating new turbocharging concepts and their impact on engine performance.

Details of the combustion models will be first given in this paper, followed by a comprehensive model validation in different engines. In particular, a premixed combustion model based on the flamelet assumption will be used to simulate the natural gas engine considering the equivalence air-fuel ratio (ϕ), spark timing, and load sweeps; a constant Equivalence Ratio Multi-Zone Approach for diffusion flames will be validated along the nominal operating curve in a Diesel engine. Different turbocharging concepts will be investigated and compared to optimize the air supply system for Diesel mode and

ammonia gas mode to enable optimal performance in both operation modes. It is important to highlight that in ammonia gas mode, diesel-pilot ignition will be replaced with spark ignition to simplify combustion modeling. This assumption should be adequate for such preliminary assessment on turbocharging systems, especially at high loads, where the diesel energy ratio is generally kept as low as possible [4], [11].

2. Combustion models

2.1. Multi-Zone Approach for Diffusion Flames

The model is based on the solution of the mixing process of the injected fuel into the trapped mass inside the cylinder by applying the momentum jet theory developed by Musculus and Kattke [12]. The computed mixing distributions are casted into a pre-defined number of zones characterized by constant equivalence ratios in which the combustion process takes place. As a result, the model is able to predict the ignition of the charge in Diesel engines which depends on both physical aspects, such as fuel evaporation and charge distribution, and chemical kinetics. Real engine conditions and geometry sub-models are included: the geometrical details of the combustion chamber, the characteristics of the injection system, and the charge thermodynamic conditions such as in-cylinder pressure, temperature, and presence of EGR are considered.

The model can be split into two sub-models, a one-dimensional charge stratification one used to describe the direct injection of liquid fuel from which the mass and energy exchanges between the homogeneous iso-ϕ zones are computed through a 2D resolution of the reacting fuel spray. This information is later used in a zero-dimensional combustion model that computes the multi-zone properties, including combustion and emission formation processes [13].

Charge stratification model and coupled chemical-physical ignition

In the extension of the momentum jet theory developed by Musculus and Kattke [12], a conical numerical spray domain is divided into small control volumes (as shown in Figure 1) with a fixed axial width Δz, whose value can be arbitrarily chosen and is set to 0.001 m in this study. Initially, these CVs are filled by air.

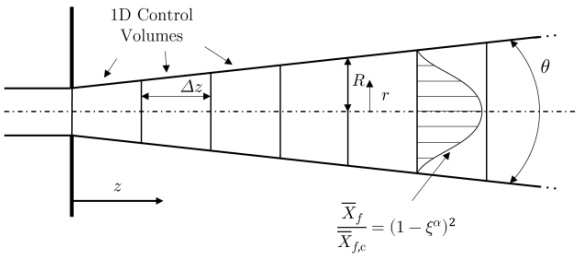

Figure 1: 1D discretization of the fuel spray in axial control volumes. Details of the spreading angle θ, iso-ϕ contours and radial distribution are illustrated.

The cone spray angle of the one-dimensional domain is computed with the formulation proposed by Naber et al in [14]:

$$\theta = 2 \cdot arctan\left[C_\theta \left(\left(\frac{\rho_a}{\rho_f}\right)^{0.19} - 0.0043\left(\frac{\rho_f}{\rho_a}\right)^{0.5}\right)\right] \quad (1)$$

Where ρ_a and ρ_f are the ambient air and liquid fuel density, C_θ is a tuning parameter specific to geometry of the injector. These quantities are determined at the Start Of Injection (SOI) and kept constant during the simulation. Following an Eulerian approach, the variation of the mass of fuel and total jet momentum at each time step for a given CV are computed with:

$$\frac{dm_f}{dt} = \dot{m}_{f,in} - \dot{m}_{f,out} \tag{2}$$

$$\frac{dM}{dt} = \dot{M}_{in} - \dot{M}_{out} \tag{3}$$

Where m_f and M are the mean axial turbulent fuel mass and jet momentum, respectively. Over-dots quantities indicate integral flux quantities, with subscripts denoting whether the contribution is entering or exiting the CV. From these equations, it is possible to obtain the fuel distribution in the iso-equivalence ratios zone by imposing a radial distribution of fuel in each CV. Further information on the application of this post-process of the 1D spray model can be found in [9], [15]. The interaction of the spray with the wall (piston or liner) is also accounted for as it greatly affects the combustion process. In particular, after the so-called POI (Point Of Impact), the cone spray angle is reduced and the radial distribution is changed to account for the "packing" of the leanest particles with the ones deviating from the core to the edge of the spray by the impact with the piston walls. This results in a lower air entrainment and the subsequent reduction of the heat released by combustion, which is typical of diffusive combustion processes. In addition, the spray model includes specific sub-models to simulate the coupled chemical-physical ignition mechanism. Indeed, the physical aspect is considered by classifying the CVs that form the 1D spray into three sub-regions, namely "liquid", "unburned vapor" and "burned vapor. The "liquid" sub-region is defined via a thermodynamic evaporation sub-model based on the hypothesis of mixing-controlled evaporation [16], [17]. With this model, it is possible to identify the Liquid Length (LL), as the one-dimensional threshold between the "liquid" and "vapor" region of the spray. Downstream the LL, the fuel is assumed to be in the "vapor" state and ready to react. To compute the actual ignition, which is delayed by chemical kinetics, the Tabulated Kinetics Ignition (TKI) approach is developed, providing a detailed and fast description of the complex reaction mechanisms [18], [19]. This approach is based on the computation of a normalized progress variable c along the axial control volumes. Ignition occurs when $c_i \geq c_{i,ign}$ in one of the CVs. After this, the status of that CV will be updated from "unburnt vapor" to "burned vapor" and combustion has started. It is also possible to identify the Flame Lift-off Length (FLOL) as the closest CV to the injector in a "burnt vapor" state. A conceptual description of the 1D spray and division in the three different sub-regions is shown in Figure 2.

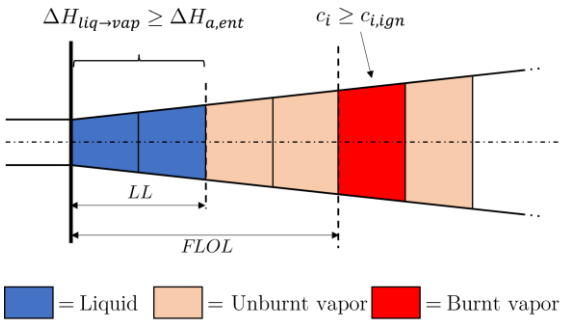

Figure 2: Scheme of the "liquid", "unburned vapor" and "burned vapor" state sub-regions in the 1D spray domain.

Computational scheme of the model

The computational scheme implemented for this model is subdivided into the following steps:

1. The conditions at IVC, including pressure, temperature, and compositions, are used as initial conditions for combustion simulation.
2. Before the SOI, a single zone containing only the fresh charge is considered. The in-cylinder pressure and temperature are computed at each iteration, taking into account only the heat exchange with the walls and the compression of the charge due to piston motion.
3. Once the injection starts, the 1D CV approach is used to determine the spatial distribution of the iso-ϕ zones. The newly created thermodynamic zones are populated, and for each zone, the mass, temperature, composition, and other thermodynamic quantities are calculated. A homogeneous pressure is assumed for the entire cylinder and all zones.
4. The evolution of the spray is performed for each CV. Each CV will contain either the liquid fuel or the "vapor" mixture in the "unburned" or "burned" state. For the CVs in the "vapor" state, the progress variable c_i is calculated to determine where the ignition occurs first and to identify the "burnt" and "unburnt" CVs.
5. If combustion has started, the thermodynamic properties are recomputed. It is necessary to consider that for each "vapor" CV two states ("burnt" and "unburnt") can coexist, so the energy balance must be written for each zone. The derivatives of the "burnt" zones need to include the heat released by the combustion of the fresh charge. Moreover, the NO emissions are calculated with a Zeldovich-extended thermal mechanism [20], [21] as described in [9].
6. Steps 2 to 5 are repeated until the Exhaust Valve Opening (EVO) is reached.

2.2. Premixed combustion model based on flamelet assumption

The objective of predictive combustion models within the 0D approaches is to sufficiently describe the influence of the main physical and chemical parameters that determine the overall burning rate, despite the simplifications introduced by the inability to resolve the flow field locally:

- at the spark timing, a high-temperature kernel of the order of 1 mm in diameter between the electrodes of the sparkplug is formed. The growth of its initial flame kernel is quasi-laminar and highly stretched with a gradual transition to a turbulent flame as the local flow increasingly distorts the flame front;
- when the flame is fully developed, turbulence wrinkles considerably the flame front, and the flame propagates throughout the combustion chamber, where the greatest part of the energy content is released. Microscopically examining the globally wrinkled and turbulent flame reveals that its structure remains laminar and its thickness consistently thin, characteristic of a corrugated flame or wrinkled flamelets combustion regime. Hence every element of the flame propagates toward the fresh gases with the laminar flame speed, so that the burning rate would depend on such a flame velocity to the contour that is referred as the turbulent flame surface (A_T). Applying the Damköhler hypothesis we can correlate the ratio of the turbulence (s_T) to laminar flame speed (s_L) to the ratio of the turbulent to the mean flame surface, a contour of a fictitious mean flame surface (A_L) assumed to be spherical:

$$\frac{s_T}{s_L} = \frac{A_T}{A_L} \tag{4}$$

- turbulent flame propagation continues until flame-wall interaction becomes significant, initiating extinction mechanisms until the flame is extinguished. During this phase, flame front wrinkling diminishes due to the impact of the flow boundary layer, increased heat losses to the cold wall, and the flame's confinement by the wall.

The proposed 0D model aims to describe all these phases of the combustion process from the kernel formation to the flame extinguishment, using several sub-models to account for laminar flame speed, flame surface, aerodynamic turbulence, turbulent flame propagation, flame-wall interaction. All length scales of aerodynamic turbulence are assumed to be larger than the flame front thickness (flamelet regime), so a global turbulent flame speed or a wrinkling factor is calculated, based on a revised version of the Eddy Burn Up model, which assumes the combustion mechanism in the SI engine depends on the entrainment of turbulent eddies in the flame front.

Modified Eddy Burn Up model

Combustion is modelled in two steps: first, the fresh gases are entrained in the flame front at a speed corresponding to the turbulent flame speed (s_T). Then, the entrained mass burns over characteristic time:

$$\frac{dm_{ent}}{dt} = \rho_u A_L s_T \tag{5}$$

$$\frac{dm_b}{dt} = \frac{m_{ent} - m_b}{\tau_b} \tag{6}$$

where τ_b is a characteristic time that physically corresponds to the time required for the turbulence eddies to be entrained into the flame front. To account for the effects of variations in the burning rate with the existing turbulence intensity as a function of the engine load and speed, a modified definition of the characteristic time τ_b has been adopted:

$$\tau_b = \frac{0.15}{C_{centr}} \frac{L_i}{u'} \tag{7}$$

Where u' is the turbulent intensity and L_i is the integral length scale. The fully turbulent flame speed S_T can be determined using Gulder's correlation [22]:

$$S_T = C_{st} S_L \left(1 + 0.62 f \sqrt{\frac{u'}{S_L} Re_\eta} \right) \tag{8}$$

where C_{st} is a tuning constant and its default value is 1.0. f is a transition function from laminar (0) to turbulence (1) condition and Re_η is the Kolmogorov Reynolds number and τ_η is the Kolmogorov time scale. These equations necessitate solving for the turbulent flow field, which will be described in the following section.

Additionally, it is necessary to account for both the initial phase of combustion, involving the transition from the laminar to the fully turbulent speed, and the final phase of combustion, involving the flame-wall interaction. The initial phase is described by the introduction of a transition parameter f ($0 \leq f \leq 1$), which is computed using the Herweg and Maly approach [23]:

$$f = \left[1 - exp\left(-\frac{r_K - S_{tay}}{C_{delay} L_i}\right)\right]^{0.5} \left[1 - exp\left(-\frac{u' + S_L}{L_i} t_{ign}\right)\right]^{0.5} \quad (9)$$

where t_{ign} is the time elapsed from sparking timing, r_K is the flame kernel radius, and S_{tay} is the Taylor micro-scale. C_{delay} is a tuning constant with a default value of 1.

The end of combustion, involving flame-wall interaction, is not described by a physical model since the mechanism depends on the local structure of the flame and flow fields. Hence a phenomenological approach is used by imposing a correction factor C_w (ranging from 0 for an undisturbed flame to 1 for a quenching flame), which is computed according to a S-shape formula:

$$C_w = 1 - exp\left(-2.908 \frac{X_b - X_{b50}}{1 - X_{b50}}\right)^{2.5} \quad (10)$$

where X_b is the burnt mass fraction and X_{b50} is the burnt mass fraction when the flame surface wetted by the cylinder walls equals to 50% of the total flame front.

For all the fuels considered by the model, the Metghalchi & Keck formula [3] [4] is adopted to determine the laminar flame speed, with specific coefficients that are fuel-dependent. This correlation uses the following form to express the influence of equivalence ratio, pressure, temperature, and residual gas content:

$$S_L(\emptyset, p, T, X_{res}) = S_{L0} \left(\frac{T}{T_0}\right)^{\alpha} \left(\frac{p}{p_0}\right)^{\beta} (1 - 2.1 X_{res}) \quad (11)$$

Where the coefficients α and β depend on the fuel and the equivalence ratio. In the case of NH_3/H_2 blends, the correlation from Pessina et al. [26] is used.

In-cylinder turbulence

Turbulence inside the cylinder is primarily formed during the intake phase when the incoming air generates flow structures with large-scale turbulent motions which then expand and transform their kinetic energy into internal energy of the surroundings. As previously described, the determination of the burning mass rate requires the knowledge of the main turbulence parameters, specifically the turbulent intensity u' and the integral length L_i. In the literature, numerous approaches have been proposed, generally involving the application of Reynolds-averaged Navier-Stokes equations in quasi-dimensional simulation to model turbulence production and dissipation. Among those, here the so-called $K - k - \varepsilon$ model proposed by Fogla et al. [27] has been adopted, which accounts for the balance equation for the mean kinetic energy $K = \frac{1}{2} U^2$ (U is the mean velocity inside the cylinder), for the turbulent kinetic energy $k = \frac{3}{2} u'^2$ and for the turbulent dissipation rate ε:

$$\frac{d(mK)}{dt} = C_{in}(1 - \alpha_{in}) E_{in} + K \dot{m}_{out} - P_k \quad (12)$$

$$\frac{d(mk)}{dt} = C_{in} \alpha_{in} E_{in} + k \dot{m}_{out} + P_k + C_{tumb} T - m\epsilon \quad (13)$$

$$\frac{d(m\varepsilon)}{dt} = C_{in} E_{in} \frac{\sqrt{k}}{L_g} + \varepsilon \dot{m}_{out} + P_\varepsilon + C_{tumb} T \frac{\sqrt{k}}{L_g} - 1.92 \frac{m\varepsilon^2}{k} \quad (14)$$

where $E_{in} = (1 - C_T)\frac{1}{2}\dot{m}_{in}v_{in}^2$, $\dot{m}_{in}$ and v_{in} are the mass flow rate and isentropic velocity of the flow entering the cylinder respectively. C_T is the tumble coefficient associated with the valves. C_{in} is the model parameter which is used to account for the actual flow velocities through the valves, α_{in} is indicative of the fraction of inflow energy that directly enters the cylinder as turbulence and is not generated by the cascade process, $\dot{m}_{out}$ is the mass flow rate of the flow exiting the cylinder, T is the production of turbulence due to the decay of the tumble macro-vortex during the compression stroke and C_{tumb} is a tuning constant that controls the intensity of this process. P_k and P_ε model the production of turbulent kinetic energy and dissipation rate from the large-scale mean flows via the energy cascade process, and L_g is the angular momentum. A detailed description of each term and the validation of the model can be found in [27]. Solutions of k and ε allow to determine the turbulence intensity u' and the integral length L_i which are required to determine the burning rate applying the previously described combustion model.

Finally, pollutant emissions are determined based on equilibrium assumptions of the main species (whose list will depend on the chosen fuel) and a kinetically controlled formation of the NOx according to the well-known thermal mechanism.

3. Experimental validation

3.1. Diesel Cycle

The validation of the diffusion combustion model was first performed in a 6-cylinder medium-speed Diesel engine with a bore size of 0.2 m for marine applications, which is of interest as a conventional propulsion system to be eventually considered as a reference baseline case. The available experimental data refer to a load sweep along the nominal engine speed of 1000 rpm. While detailed information regarding the fuel injection rate profile was not available, a profile was taken from [28], scaled based on injection pressure by keeping the same ramp-up and ramp-down slopes.

Figure 3 shows the comparison between measured and computed normalized in-cylinder pressure and apparent heat release rate (AHRR). For all conditions, the model shows a rather good accuracy in describing the evolution of the combustion process, including the initial ramp of the AHRR, its quasi-steady-state value at full load, the time of its earlier decrease at lower loads, and the burnout phase. Some differences can be observed in the initial stage of combustion where experimentally a peak of heat release rate associated with premixed combustion occurs. The lack of such detail in the model is due to the use of a simplified approach for prediction ignition instead of using the Tabulated Kinetics Ignition (TKI) approach. In this work, ignition was computed for each iso-ϕ zone using the following equation:

$$\tau_{ID,y} = C_{ID}\, p_{cyl}^{-1.02} \phi_y^{-0.2} \exp\left(-\frac{E_A}{RT_{cyl}}\right) \tag{15}$$

where C_{ID} is a frequency parameter, E_A is the energy of activation and R is the gas constant. Here: $C_{ID} = 3.45\ ms^{-1}$ and $E_A/R = 2100\ K$.

During the ignition delay time, p_{cyl} and T_{cyl} may vary due to the compression resulting from piston motion. To account for these changing conditions, the ignition delay is obtained numerically by integrating the reciprocal of the equation (15) until the following relation is satisfied:

$$\int \frac{1}{\tau_{ID,y}} dt = 1 \tag{16}$$

Equation (16) has been developed under the assumption of multi-zone/two-zone combustion, a thermodynamic model often used to simulate Diesel combustion. Under these conditions, the equivalence ratio term $\phi_y^{-0.2}$ corresponds to the global air-fuel injected ratio, but in this model, it represents the local value, and its applicability is a bit more limited. The use of a TKI overcomes these limits and allows us to consider the effect of the fuel sensitivity on the ignition process, but its application was considered beyond the scope of this work and the reader is referred to other papers for these model capacities [13].

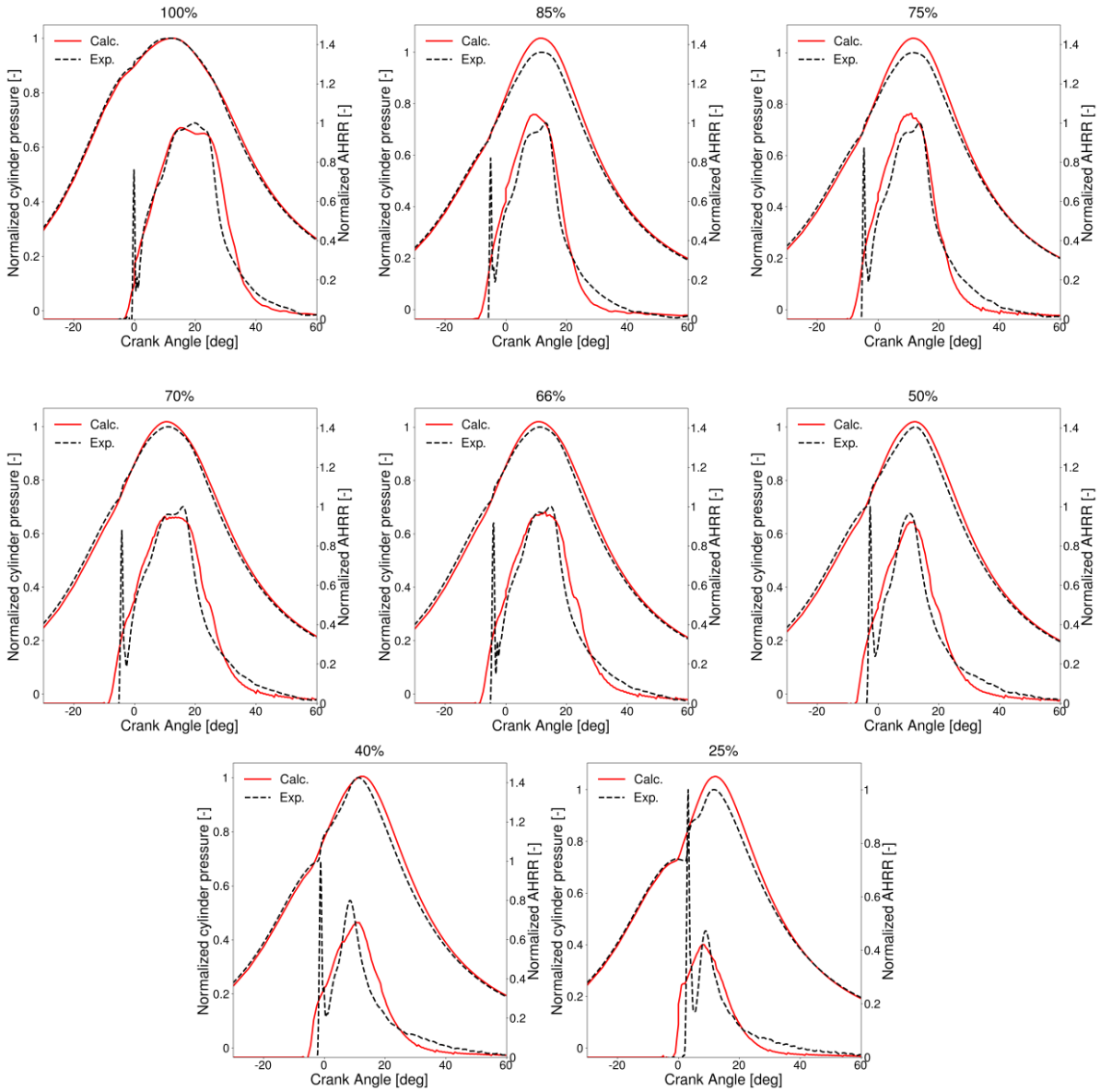

Figure 3: Comparison between experimental and computational pressure and AHRR. Results are normalized using the maximum pressure and AHRR in experiments.

Figure 4 compares the measured and computed pressure at the intake receiver on the left y-axis, while the corresponding values of the temperature at the turbine inlet are shown on the right y-axis. These

temperature values depend on the accuracy of the combustion model, and their agreement falls within an acceptable range, allowing for reliable turbocharging studies. The pressure at the intake receiver is well captured, demonstrating the accuracy of ACTUS in turbocharging simulation.

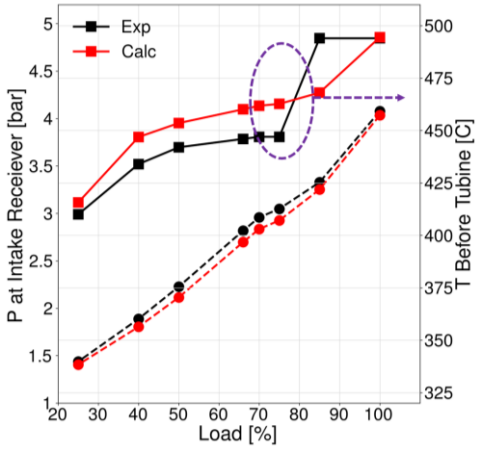

Figure 4: Comparison between measured and simulated pressure at intake receiver and temperature at turbine inlet.

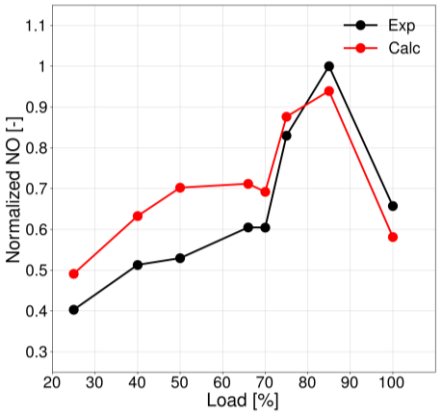

Figure 5: Comparison between measured and simulated NO_x emission. Results are normalized with respect to the maximum measured value.

Figure 5 compares the measured and simulated engine-out NO_x emissions, normalized to the maximum measured value. It demonstrates that the mode can well capture both the trend and the absolute value of NO_x emission.

3.2. Otto Cycle

The model's capabilities in describing the combustion process in spark-ignition (SI) engines were initially verified by studying a natural gas spark-ignited engine with a bore size of 0.145 m. The nominal engine speed was set at 1500 rpm, and three loads with three different spark timings (-15, -10, -5 CA aTDC) for each load and corresponding air-fuel ratio values were considered (see Table 1).

Table 1. Operating conditions

Load1	Spark Advance	λ	Load2	Spark Advance	λ	Load3	Spark Advance	λ
A1	-15 CA aTDC	1.404	**B1**	-15 CA aTDC	1.493	**C1**	-15 CA aTDC	1.518
A2	-10 CA aTDC	1.36	**B2**	-10 CA aTDC	1.418	**C2**	-10 CA aTDC	1.612
A3	-5 CA aTDC	1.305	**B3**	-5 CA aTDC	1.349	**C3**	-5 CA aTDC	1.373

Figure 6 compares the normalized measured and computed in-cylinder pressure curves and the corresponding AHRR for all three loads. For Load 1, the results show a very good agreement between measured and computed data: the model accurately predicts the compression curve, the start of combustion, the transition from laminar to turbulent combustion, the timing and value of the maximum heat release rate, and the completion of the process. The model captures the observed trend of reduced spark advance: a shift in the AHRR curves and a slight increase in their peak. Some differences between measured and computed AHRR can be observed in the last part of the combustion where the simulations show some overestimations. It is believed that in this phase of combustion, when the flame front approaches the walls, the approximations due to the sphericity of its surface become significant and the details of the occurring process cannot be completely captured due to the inherent simplifications in the approach.

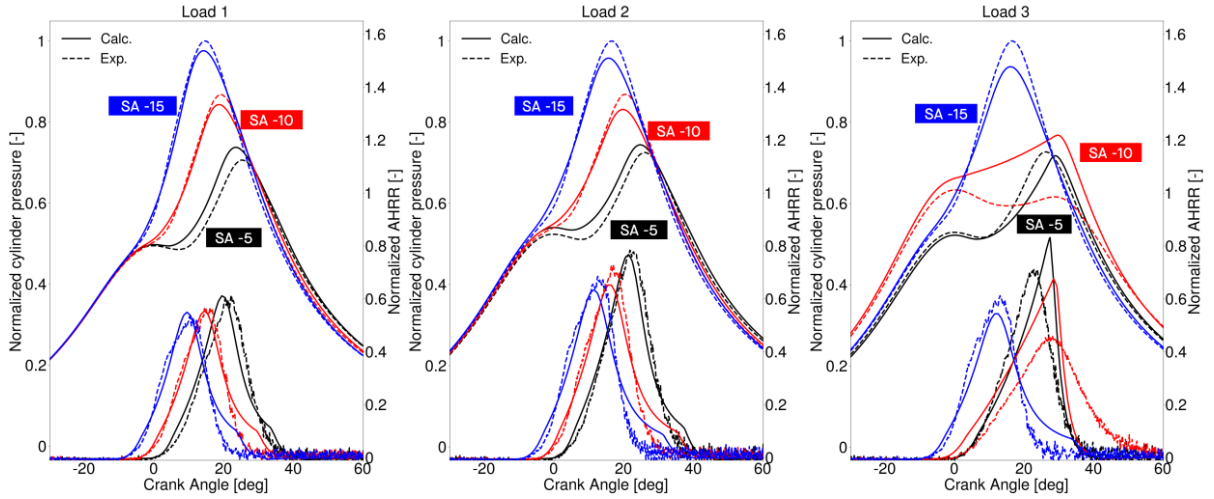

Figure 6: Comparison between measured and simulated pressure and AHRR at different loads and spark timing. Results are normalized with the maximum pressure and AHRR at different loads.

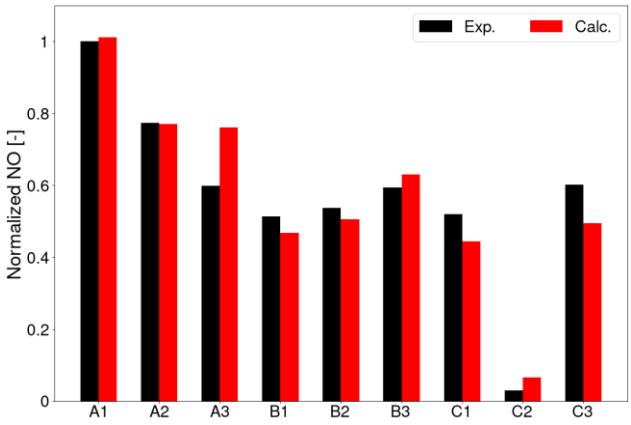

Figure 7: Comparison between measured and simulated NOx emission at different operating conditions. Results are normalized with the maximum measured value.

Similar observations can be made for Load 2, confirming the model's capabilities in this condition. At the highest load (Load 3), a good agreement in terms of the AHRR is observed for the operating points with -15 and -5 CA spark advances, with only minor differences in the computed maximum value of AHRR. However, the computed pressure curve for a spark advance of -10 CA aTDC does not align well with the measured data. Despite this, a closer examination of the AHRR profiles reveals that the model accurately captures the trend changes with varying spark advances. Specifically, the timing of the peak AHRR is delayed in the red curves (SA = -10 CA aTDC) compared to the black curve (SA = -5 CA aTDC), which is correctly represented by the model.

Figure 7 compares the measured and simulated NO_x emissions across all operating conditions. The results, normalized to the maximum measured value, show good quantitative and qualitative agreement. The model accurately predicts the observed variations at each load, attributed to combinations of spark advance and air-to-fuel ratio, as well as the changes from one load to another.

4. Turbocharging strategies

Following comprehensive validation in the previous section, these two predictive combustion models were employed in turbocharging studies to develop a concept that facilitates both Diesel and ammonia gas mode operation in a marine 4-stroke engine. To reduce computational costs, the heat release rate from the complete combustion simulation was fitted to a Wiebe function and subsequently utilized in the investigation of turbocharging concepts. Simulations were conducted along the propeller curve for a 6-cylinder engine configuration with a bore size of 0.2 m. As reported in [29], the ammonia gas engine operates within a λ range of 1.1 to 1.4, depending on the H_2 blend ratio, with 2% and 6% H_2 volume fractions considered. For this study, a λ of 1.25 with an H_2 volume fraction of 2.7% (representing 2% of the energy ratio) was selected to assess air requirements and exhaust gas, thereby determining the turbocharging requirements. The turbocharging studies will be conducted in two steps:

1. Understanding the turbocharging characteristics of ammonia gas engines, highlighting their differences from conventional gas engines, and providing guidance on identifying a suitable turbocharging system for ammonia-Diesel dual-fuel engines;
2. Assessing different turbocharging concepts for the ammonia gas mode and ensuring its compatibility with the Diesel operation mode.

4.1. Ammonia gas mode turbocharging characteristics

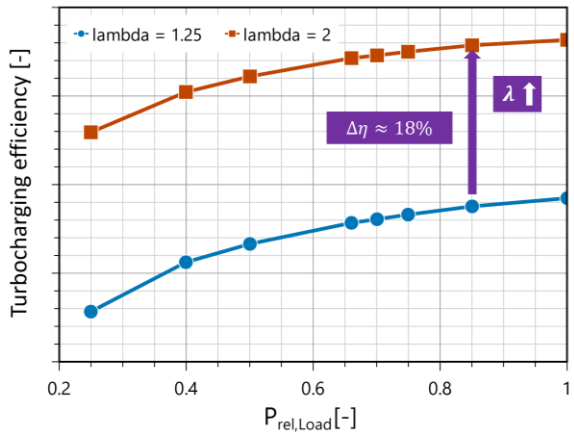

Figure 8: Turbocharging efficiency for gas engine operates at λ = 1.25 and 2.

As illustrated in Figure 8, operating under a low λ requires a lower turbocharging efficiency, which is defined by the energy ratio between the charge entering the cylinder and the exhaust gas exiting the cylinder. This is due to the high exhaust gas temperature and low inlet mass flow rate under such conditions. Compared to a commercial gas engine operating at λ ~ 2, reducing the λ to 1.25 could result in an 18% decrease in the turbocharging efficiency requirement. Consequently, a certain amount of energy must be dissipated in the turbocharging process for ammonia gas operation. Common methods to achieve this include using a wastegate and compressed air blow-off (or compressor recirculation), which will be studied and compared in the next section.

The operation lines for two fuel admission concepts—port fuel injection (PFI) and fuel admission upstream of the compressor—are illustrated in Figure 9. It is evident that under the same operating conditions, the PFI concept results in a much lower volume flow rate due to the absence of fuel in the compressed gas, which accounts for approximately 11.35% of the total mass. The fuel mass fraction is proportional to: $\frac{1}{\lambda*(stoichiometric\ AFR/LHV)}$, where stoichiometric AFR represents the stoichiometric air-fuel ratio and LHV is the low heating value. Such high fuel mass fraction in the ammonia gas engine can therefore be attributed to two factors: the low λ operation and the low stoichiometric AFR/LHV of ammonia. Specifically, ammonia has a stoichiometric AFR/LHV of 0.325, which is around 5% lower than that of methane (stoichiometric AFR/LHV $\approx$ 0.344). This suggests that the fuel admission approach could have a nonnegligible impact on turbo-matching, and detailed studies should be performed for each concept. In this study, the authors will focus only on the PFI concept.

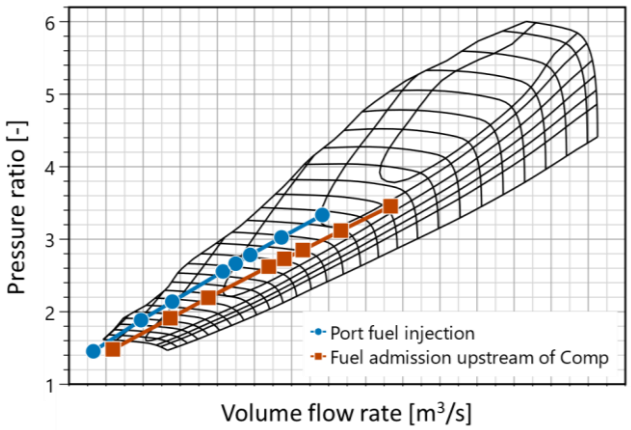

Figure 9: Operation lines for port fuel injection and fuel admission upstream of the compressor concepts.

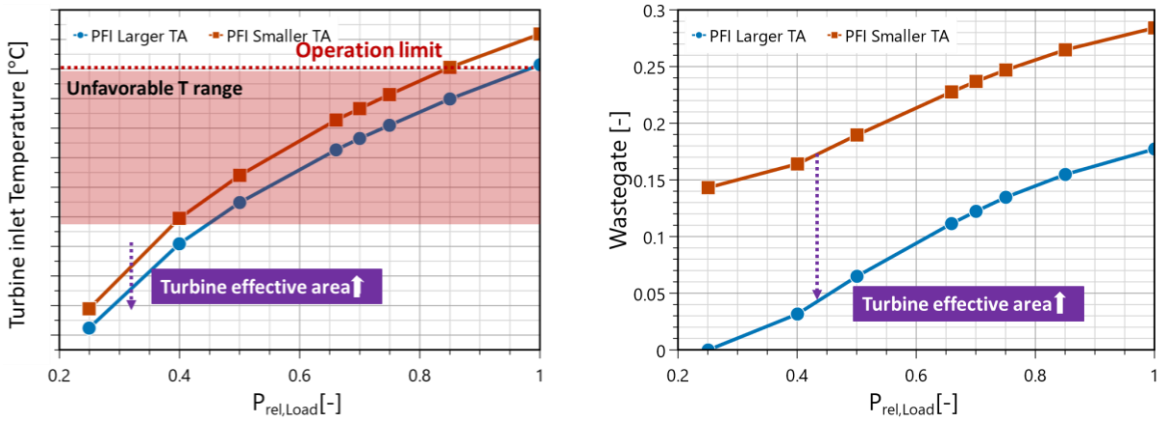

(a) Turbine inlet temperature

(b) Wastegate mass flow rate ratio

Figure 10: Effects of turbine effective area in the PFI ammonia engine.

Figure 10 illustrates the impact of increasing the turbine effective area (S_{eff}). As shown, a larger turbine can reduce the engine back pressure and improve the gas exchange phase. This results in less hot exhaust gas being trapped in the cylinder and a lower temperature at IVC, and consequently, a reduction of the turbine inlet temperature and the opening of the wastegate. However, even with the maximum feasible S_{eff}, where the wastegate is switched off at 25% load (as further increases in S_{eff} would fail to meet the low-load air requirement), the turbine inlet temperature still exceeds the component's operational limit. Most operating conditions fall within an unfavorable temperature range, where constant operation could shorten the maintenance interval. A potential solution to lower the turbine inlet temperature is to activate the engine bypass and cool the exhaust gas with air from the compressor outlet. To summarize, operating in ammonia gas mode may require:

- Compressed air blow-off or a wastegate to dissipate excess energy during the turbocharging process.
- An engine bypass to lower the turbine inlet temperature, bringing it below the component operation limit and avoiding the unfavorable temperature range.

These considerations will be studied and compared in the next section, where compatibility between Diesel and gas modes, in other words, using the same turbocharger specifications for both Diesel and gas modes, will also be taken into account.

4.2. From Diesel mode to ammonia gas mode

The turbocharger specifications were first selected for Diesel mode, where maintaining a high λ (indicative of turbocharging efficiency) is crucial to minimize soot formation. This approach leaves limited flexibility for tuning or matching the turbocharging system. In this paper, the turbine effective area was chosen to ensure the λ remains above the smoke limit at low load (λ = 1.65 at 25% load was obtained). These specifications were then applied to investigate different turbocharging concepts for ammonia gas mode. Specifically, the study assessed the wastegate with engine bypass and compressed air blow-off with engine bypass approaches, as depicted in Figure 11.

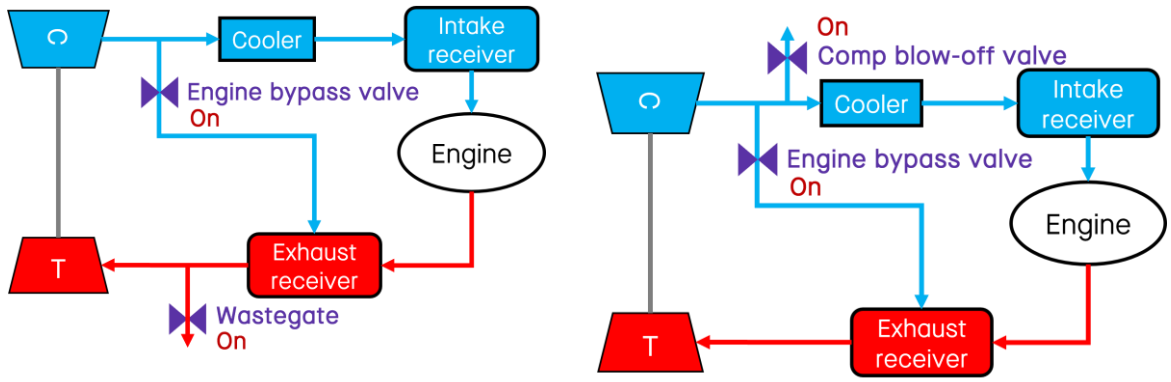

(a) Wastegate & engine bypass concept *(b) Compressed air blow-off & engine bypass concept*

Figure 11: Schematic diagram of different turbocharging concepts.

Concept 1: Wastegate & Engine bypass

Figures 12(a) and (b) respectively depict the operation lines and turbine inlet temperatures for Diesel mode and ammonia gas mode using wastegate and engine bypass turbocharging concepts, as well as the wastegate-only approach. An increase in engine bypass ratio or a wider engine bypass valve opening can result in a higher compressor volume flow rate and a lower turbine inlet temperature. Detailed operating parameters are illustrated in Figure 13: approximately 27% of the exhaust gas/energy must be dissipated through the wastegate at 100% load, with the wastegate opening reducing as the load decreases. However, the wastegate needs to remain open even at low load to maintain a low λ . As the engine bypass increases, a higher wastegate ratio becomes necessary at low loads for two reasons: the increased engine bypass elevates the energy flow in the exhaust, and the turbocharger efficiency improves (Figure 13(a)) due to the higher expansion ratio of the turbine, which shifts the operation point to a more efficient zone. An opposite trend is observed at high load (100% load), where the reduction in engine efficiency becomes more significant. This will be further discussed in Figure 14.

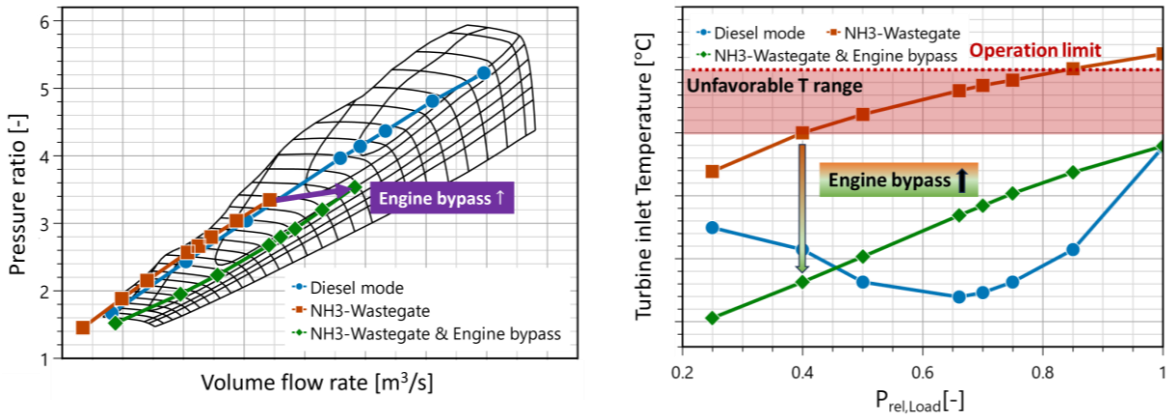

(a) Operation line *(b) Turbine inlet temperature*

Figure 12: Comparison between Diesel mode operation, and ammonia gas mode with and without engine bypass turbocharging systems.

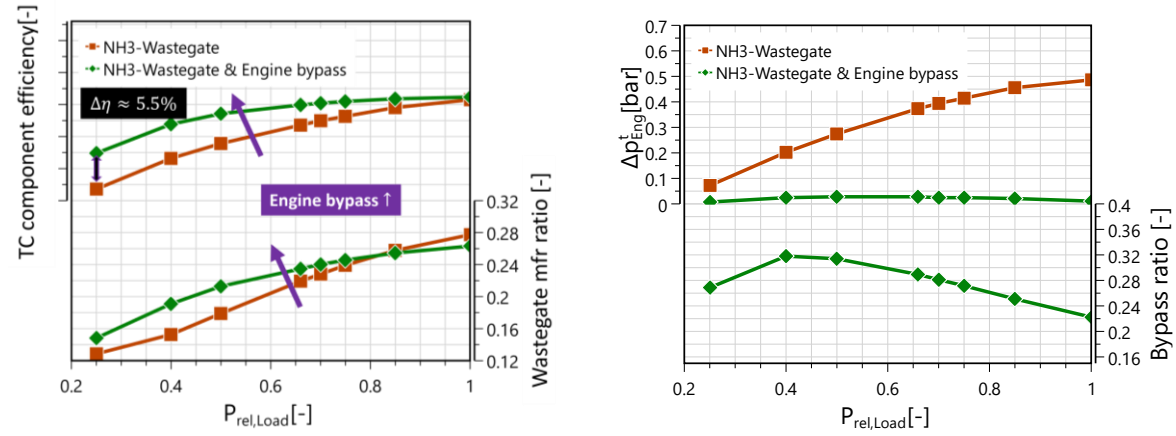

(a) Turbocharger efficiency & mass flow rate ratio *(b) Pressure difference over engine & engine bypass ratio*

Figure 13: Comparison between two turbocharging systems for ammonia gas mode operation: wastegate only vs engine bypass & wastegate.

As also shown in Figure 12(a), the operation line shifts to a more efficient zone in the compressor map. However, further increases in engine bypass may cause the operation line to approach the choke region, significantly reducing compressor efficiency, which limits the potential reduction in turbine inlet temperature. However, such an increase in engine bypass is not feasible with passive engine bypass control, as the engine bypass remains fully open at all loads, and the pressure difference across the engine (from intake to exhaust) becomes too low (around 20 mbar) to drive additional flow from intake to exhaust (Figure 13(b)). Such a small pressure difference can lead to a high gas exchange loss and consequently lower engine efficiency. As shown in Figure 14, there is approximately a 0.67%-pts loss in engine efficiency at 100% load where the pressure difference drops the most (Figure 13(b)) when changing the engine bypass opening from 0 to 100%. It is important to note that these two methods (in Figure 12(a)) represent the extreme cases, with any additional measures (e.g. pump). An intermediate option can be chosen with the appropriate wastegate ratio and bypass ratio.

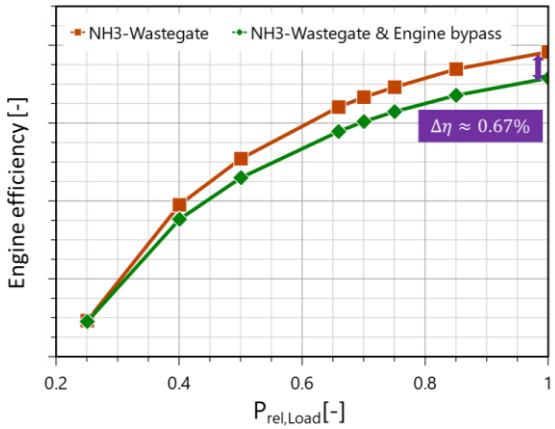

Figure 14: Comparison of engine efficiency in ammonia gas mode: wastegate only vs. engine bypass and wastegate turbocharging systems.

Concept 2: Compressed air blow-off & Engine bypass

Figure 15(a) and (b) present the operation lines and turbine inlet temperatures for Diesel mode and ammonia gas mode using the compressed air blow-off turbocharging approach. It is evident that, with compressed air blow-off alone, the turbine inlet temperature becomes too high for ammonia gas operation at most loads, necessitating the opening of the engine bypass valve. However, using compressed air blow-off results in a high volume flow rate in the compressor, and opening the engine bypass valve shifts the operation line further into the choke region. A potential solution could be the cut-in of an additional turbocharger in ammonia gas mode to facilitate the use of both compressed air blow-off and the engine bypass. The operation lines for such a turbocharger cut-in system are shown in Figure 16(a) for the main turbocharger and (b) for the additional cut-in turbocharger. The cut-in turbocharger is significantly smaller, with about 54% of the flow capacity of the main turbocharger.

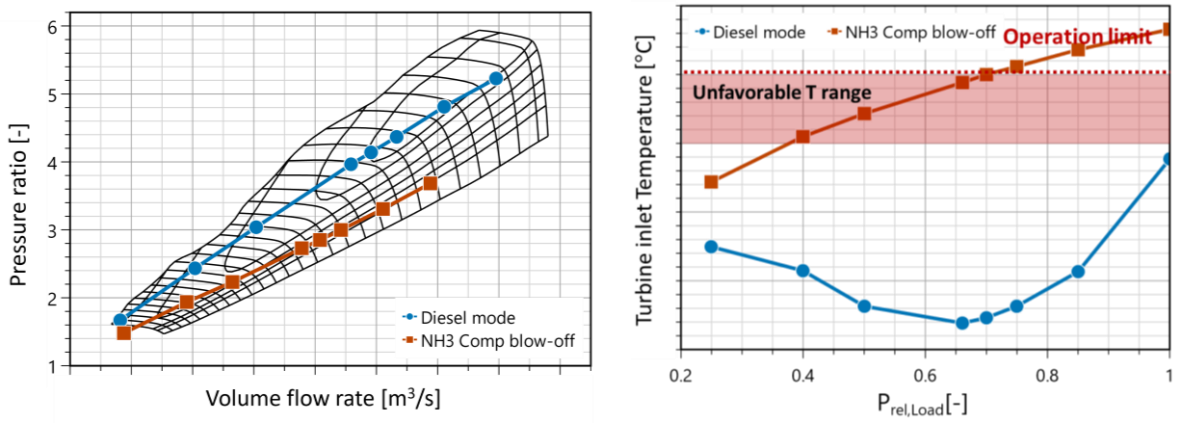

(a) Operation line

(b) Turbine inlet temperature

Figure 15: Ammonia gas mode with compressed air blow-off turbocharging system

In Figure 16(a), the operation line for the compressed air blow-off & engine bypass approach in ammonia gas mode is closer to that of the Diesel mode, indicating a more efficient compressor operation zone compared to the wastegate & engine bypass turbocharging system. Figure 17 illustrates that the turbine inlet temperatures for both Diesel and ammonia gas modes, using two different

turbocharging strategies, reveal that the compressed air blow-off with engine bypass achieves a lower turbine inlet temperature due to the higher engine bypass ratio (Figure 18(a)). As seen in Figure 16(a), there is potential for further shifting of the operation line in the compressed air blow-off & engine bypass setup, suggesting that additional adjustments to the engine bypass ratio can still be made to control the turbine inlet temperature.

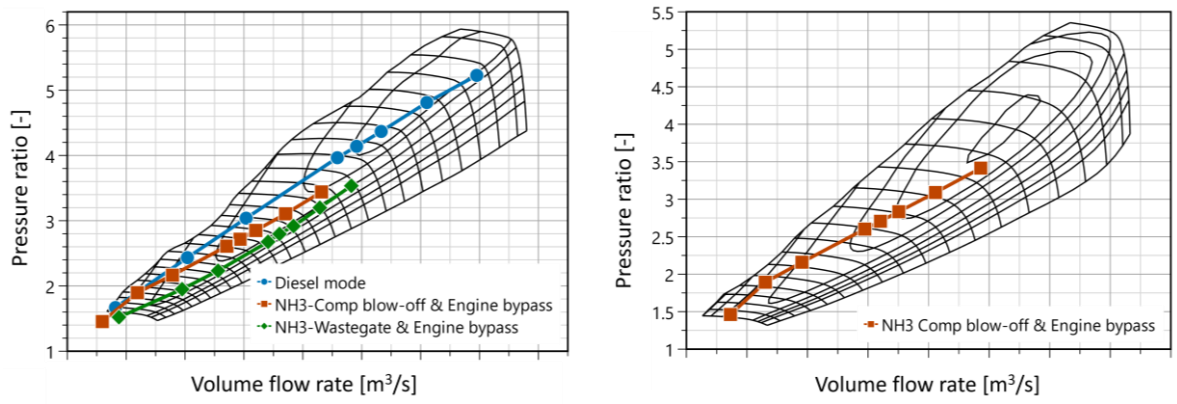

(a) Main turbocharger *(b) Cut-in turbocharger*

Figure 16: Operation lines for Diesel mode, and ammonia gas mode with two different turbocharging systems: compressed air blow-off only, and compressed air blow-off & engine bypass.

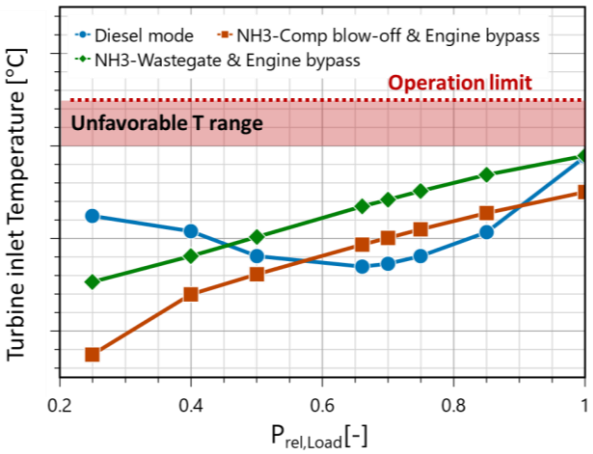

Figure 17: Temperatures at turbine inlet for Diesel mode operation, and ammonia gas mode with two different turbocharging concepts: compressed air blow-off & engine bypass and wastegate & engine bypass.

Figure 18(a) also shows that the compressed air blow-off method allows for a higher engine bypass ratio, defined by the mass flow rate through the engine bypass valve relative to the mass flow rate after the compressed air blow-off valve. This is because the turbocharger cut-in significantly reduces engine back pressure, thereby increasing the pressure difference across the engine. This results in a high mass flow rate through the bypass valve and a high bypass ratio without fully opening the bypass valve. At 25% loads, the engine bypass valve needs to be fully open to increase energy flow at the turbine inlet and achieve the target λ. Reducing the turbine effective area of the cut-in turbocharger may be beneficial at low loads, which will be investigated in future studies. Figure 18(b) presents the wastegate and compressed air blow-off ratios for each turbocharging system, showing that approximately 23% of

the compressed air or 26% of the exhaust gas needs to be dissipated at 100% load to meet the low λ requirement. Figure 19 compares the engine efficiency in ammonia gas mode using two different turbocharging systems. The compressed air blow-off approach demonstrates a slight improvement in engine efficiency due to reduced gas exchange loss resulting from higher pressure over the engine. In summary, compared to the wastegate approach, the turbocharger cut-in with compressed air blow-off has two primary functions: it provides additional control over turbine inlet temperature and converts the energy flow of exhaust gas passing through the wastegate into compressed air.

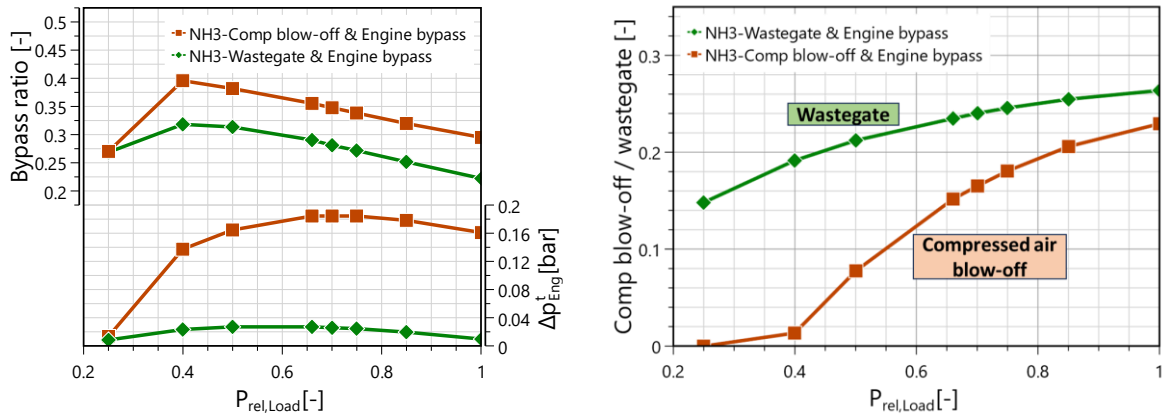

(a) Engine bypass ratio & pressure difference over engine *(b) wastegate / compressed air blow-off ratio*

Figure 18: Comparison between two turbocharging concepts for ammonia gas mode: compressed air blow-off & engine bypass vs wastegate & engine bypass.

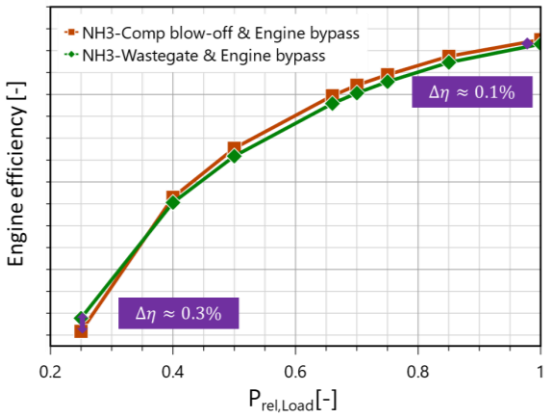

Figure 19: Comparison of engine efficiency in ammonia gas mode: compressed air blow-off & engine bypass vs wastegate & engine bypass turbocharging concepts.

5. Conclusion and outlook

This paper presents the latest development of our in-house software, which now includes advanced and predictive thermodynamic combustion models for both premixed and diffusive combustion, developed by Politecnico di Milano. A comprehensive validation was conducted to build confidence in their application for turbocharging assessments. The characteristics of ammonia gas engine turbocharging were evaluated, and various turbocharging concepts were studied and compared

considering the compatibility with Diesel mode operation. Key observations can be summarized as follows:

- The premixed and diffusion combustion models can accurately predict the combustion processes in natural gas and Diesel engines, respectively, demonstrating their reliability for turbocharging studies.
- Due to the low LHV of ammonia and the low λ operation, the fuel accounts for about 11.35% of the air-fuel mixture, indicating that the fuel admission concepts (fuel admission before or after the compressor) could have an impact on turbo-matching.
- In the ammonia gas engine, over 20% of the energy from the exhaust gas needs to be dissipated during the turbocharging process. This is necessary even using the largest feasible turbine effective area, due to the high turbine inlet temperature and low air requirement from the low λ operation and the turbine inlet temperature exceeds component limits. Wastegate or compressed air blow-off can be used to dissipate the extra energy, and the engine bypass could reduce the temperature below the operation limit of the components.
- The wastegate and engine bypass approach can enable compatibility between ammonia gas mode and Diesel mode operation, and such configuration can be found in existing gas-Diesel dual-fuel engines, making it a straightforward retrofitting solution. However, there is a trade-off between the compressor operation line and the turbine inlet temperature: a higher turbine inlet temperature brings the operation line closer to the efficient zone / Diesel mode operation line in the compressor map.
- The compressed air blow-off and engine bypass approach can also enable compatibility with Diesel mode operation and allow greater adjustment of turbine inlet temperature. However, this approach involves a turbocharger cut-in/-out process during operation, adding complexity to control, and how and where the extra compressed air can be utilized need to be explored.

Some considerations for future investigation include:

- Extending the combustion model for dual-fuel applications, incorporating the diesel pilot to achieve a more realistic turbocharging analysis for an ammonia-Diesel fuel-flexible dual-fuel engine.
- Conducting transient investigations of different control methods to facilitate a smooth transition between the two operation modes.
- Investigating the waste heat recovery in ammonia gas mode to enhance the overall energy efficiency of the ship: utilizing exhaust gas from the wastegate in the wastegate & engine bypass approach, and applying the extra compressed air in the compressed air blow-off & engine bypass approach.

Acknowledgment

The authors extend their gratitude to all colleagues within the Accelleron c/o Turbosystem Switzerland Ltd and Politecnico di Milano who contributed to the considerations and studies presented in this paper, as well as to those who participated in the discussion and revision of its content. Special thanks

to Alberto Pedrocchi, Stefan Hiltbrand, Raphael Ryser, Gilles Hardy, and Prof. Gianluca Montenegro for their significant contributions to the paper and the project.

Literature

[1] "Revised GHG reduction strategy for global shipping adopted." Accessed: Jul. 22, 2024. [Online]. Available: https://www.imo.org/en/MediaCentre/PressBriefings/pages/Revised-GHG-reduction-strategy-for-global-shipping-adopted-.aspx

[2] B. Stolz, M. Held, G. Georges, and K. Boulouchos, "Techno-economic analysis of renewable fuels for ships carrying bulk cargo in Europe," *Nat. Energy*, vol. 7, no. 2, pp. 203–212, Feb. 2022, doi: 10.1038/s41560-021-00957-9.

[3] F. M. Kanchiralla, S. Brynolf, T. Olsson, J. Ellis, J. Hansson, and M. Grahn, "How do variations in ship operation impact the techno-economic feasibility and environmental performance of fossil-free fuels? A life cycle study," *Appl. Energy*, vol. 350, p. 121773, Nov. 2023, doi: 10.1016/j.apenergy.2023.121773.

[4] X. Zhou, T. Li, N. Wang, X. Wang, R. Chen, and S. Li, "Pilot diesel-ignited ammonia dual fuel low-speed marine engines: A comparative analysis of ammonia premixed and high-pressure spray combustion modes with CFD simulation," *Renew. Sustain. Energy Rev.*, vol. 173, p. 113108, Mar. 2023, doi: 10.1016/j.rser.2022.113108.

[5] A. J. Nyongesa, J. K. Kim, and W.-J. Lee, "Investigation on the combustion of ammonia using direct high/medium-pressure-Otto injection approach in a diesel two-stroke marine slow speed engine," *J. Energy Inst.*, vol. 114, p. 101641, Jun. 2024, doi: 10.1016/j.joei.2024.101641.

[6] "Dual-fuel engines from Wärtsilä," Wartsila.com. Accessed: Jul. 22, 2024. [Online]. Available: https://www.wartsila.com/encyclopedia/term/dual-fuel-engines-from-wartsila

[7] N. Watson, A. D. Pilley, and M. Marzouk, "A Combustion Correlation for Diesel Engine Simulation," SAE International, Warrendale, PA, SAE Technical Paper 800029, Feb. 1980. doi: 10.4271/800029.

[8] V. D. Bellis, F. Bozza, D. Tufano, V. D. Bellis, F. Bozza, and D. Tufano, "A Comparison Between Two Phenomenological Combustion Models Applied to Different SI Engines," presented at the International Powertrains, Fuels & Lubricants Meeting, SAE International, Oct. 2017. doi: 10.4271/2017-01-2184.

[9] M. Tamborski, G. D'Errico, T. Lucchini, T. Cerri, and A. Onorati, "A Constant Equivalence Ratio Multi-Zone Approach for a Detailed and Fast Prediction of Performances and Emission in CI Engines," *SAE Int. J. Adv. Curr. Pract. Mobil.*, vol. 4, no. 5, Art. no. 2022-01–0381, Mar. 2022, doi: 10.4271/2022-01-0381.

[10] "Turbo boost: ACTUS is ABB's new simulation software for large turbocharged combustion engines," ResearchGate. Accessed: Jul. 22, 2024. [Online]. Available: https://www.researchgate.net/publication/296067793_Turbo_boost_ACTUS_is_ABB's_new_simulation_software_for_large_turbocharged_combustion_engines

[11] Y. Qiu *et al.*, "Ammonia fueled engine with diesel pilot ignition: Approach to achieve ultra-high ammonia substitution," *Int. J. Engine Res.*, p. 14680874241248507, Apr. 2024, doi: 10.1177/14680874241248507.

[12] M. P. B. Musculus and K. Kattke, "Entrainment Waves in Diesel Jets," *SAE Int. J. Engines*, vol. 2, no. 1, Art. no. 2009-01–1355, Apr. 2009, doi: 10.4271/2009-01-1355.

[13] M. Tamborski, G. D'Errico, T. Lucchini, and A. Onorati, "Detailed prediction of HRR and NOx emissions in CI engines via a novel thermodynamic model with constant equivalence ratio zones," *Int. J. Engine Res.*, vol. 24, no. 6, pp. 2315–2337, Jun. 2023, doi: 10.1177/14680874221128645.

[14] J. D. Naber, D. L. Siebers, J. D. Naber, and D. L. Siebers, "Effects of Gas Density and Vaporization on Penetration and Dispersion of Diesel Sprays," presented at the International Congress & Exposition, SAE International, Feb. 1996. doi: 10.4271/960034.

[15] A. Ballerini *et al.*, "Extension and Validation of a Constant Equivalence Ratio Multi-Zone Approach to DME Combustion in Vessels and CI Engines," presented at the WCX SAE World Congress Experience, SAE International, Apr. 2023. doi: 10.4271/2023-01-0193.

[16] D. L. Siebers, "Scaling Liquid-Phase Fuel Penetration in Diesel Sprays Based on Mixing-Limited Vaporization," presented at the International Congress & Exposition, SAE International, Mar. 1999. doi: 10.4271/1999-01-0528.

[17] D. L. Siebers, "Liquid-Phase Fuel Penetration in Diesel Sprays," *SAE Trans.*, vol. 107, pp. 1205–1227, 1998.

[18] Q. Zhou, T. Lucchini, G. D'Errico, G. Hardy, and X. Lu, "Modeling heavy-duty diesel engines using tabulated kinetics in a wide range of operating conditions," *Int. J. Engine Res.*, vol. 22, no. 4, pp. 1116–1132, Apr. 2021, doi: 10.1177/14680874198961 65.

[19] T. Lucchini, D. Pontoni, G. D'Errico, and B. Somers, "Modeling diesel combustion with tabulated kinetics and different flame structure assumptions based on flamelet approach," *Int. J. Engine Res.*, vol. 21, no. 1, pp. 89–100, Jan. 2020, doi: 10.1177/1468087419862945.

[20] R. Miller, G. Davis, G. Lavoie, C. Newman, and T. Gardner, "A Super-Extended Zel'dovich Mechanism for No x Modeling and Engine Calibration," *SAE Trans.*, vol. 107, pp. 1090–1100, 1998.

[21] I. B. Zeldovich, G. I. Barenblatt, V. B. Librovich, and G. M. Makhviladze, "Mathematical theory of combustion and explosions," Jan. 1985, Accessed: Jun. 17, 2024. [Online]. Available: https://www.osti.gov/biblio/6082197

[22] Ö. L. Gülder, "Correlations of Laminar Combustion Data for Alternative S.I. Engine Fuels," presented at the West Coast International Meeting and Exposition, SAE International, Aug. 1984. doi: 10.4271/841000.

[23] R. Herweg and R. R. Maly, "A Fundamental Model for Flame Kernel Formation in S. I. Engines," SAE International, Warrendale, PA, SAE Technical Paper 922243, Oct. 1992. doi: 10.4271/922243.

[24] M. Metghalchi and J. C. Keck, "Laminar burning velocity of propane-air mixtures at high temperature and pressure," *Combust. Flame*, vol. 38, pp. 143–154, Jan. 1980, doi: 10.1016/0010-2180(80)90046-2.

[25] M. Metghalchi and J. C. Keck, "Burning velocities of mixtures of air with methanol, isooctane, and indolene at high pressure and temperature," *Combust. Flame*, vol. 48, pp. 191–210, Jan. 1982, doi: 10.1016/0010-2180(82)90127-4.

[26] V. Pessina, F. Berni, S. Fontanesi, A. Stagni, and M. Mehl, "Laminar flame speed correlations of ammonia/hydrogen mixtures at high pressure and temperature for combustion modeling applications," *Int. J. Hydrog. Energy*, vol. 47, no. 61, pp. 25780–25794, Jul. 2022, doi: 10.1016/j.ijhydene.2022.06.007.

[27] N. Fogla, M. Bybee, M. Mirzaeian, F. Millo, and S. Wahiduzzaman, "Development of a K-k-∈ Phenomenological Model to Predict In-Cylinder Turbulence," *SAE Int. J. Engines*, vol. 10, no. 2, Art. no. 2017-01–0542, Mar. 2017, doi: 10.4271/2017-01-0542.

[28] K. Panagiotis, "The effects of prolonged ignition delay due to charge air temperature reduction on combustion in a diesel engine," Ph.D. dissertation, ETH Zurich, 2013. [Online]. Available: https://www.research-collection.ethz.ch/bitstream/handle/20.500.11850/70618/eth-7278-02.pdf

[29] "E-Fuels als Schlüsseltechnologie der Dekarbonisierung." [Online]. Available: https://www.jenbacher.com/images/medias/files/6376/sonderdruck_mtz_innio__2024_deutsch_final2.pdf

[30] A. Valera-Medina, H. Xiao, M. Owen-Jones, W. I. F. David, and P. J. Bowen, "Ammonia for power," *Prog. Energy Combust. Sci.*, vol. 69, pp. 63–102, Nov. 2018, doi: 10.1016/j.pecs.2018.07.001.